Research Square

Preprints are preliminary reports that have not undergone peer review.
They should not be considered conclusive, used to inform clinical practice,
or referenced by the media as validated information.

Temozolomide (TMZ) Inhibits Glioma Cell Proliferation by Inducing Ferroptosis: Effect and Mechanism

Jianglong Yu

yujianglong@xjmu.edu.cn

Xinjiang Medical University

Abudula Aisha

Xinjiang Medical University

Yan Yang

The Second Affiliated Hospital of Xinjiang Medical University

Xinping Luan

The Second Affiliated Hospital of Xinjiang Medical University

Xu Zhang

The Second Affiliated Hospital of Xinjiang Medical University

Yongji Zhu

The Second Affiliated Hospital of Xinjiang Medical University

Research Article

Keywords: Glioma, TMZ, GSH, GPX4, Ferroptosis, ROS

Posted Date: May 27th, 2026

DOI: https://doi.org/10.21203/rs.3.rs-9740279/v1

License: This work is licensed under a Creative Commons Attribution 4.0 International License.
Read Full License

Additional Declarations: No competing interests reported.

Temozolomide (TMZ) Inhibits Glioma Cell Proliferation by Inducing Ferroptosis: Effect and Mechanism

Jianglong Yu[1, 2*], Abudula·Aisha[1, 2], Yan Yang[2], Xinping Luan[2], Xu Zhang[2], Yongji Zhu[2]

[1] State Key Laboratory of Pathogenesis, Prevention and Treatment of High Incidence Diseases in Central Asia, Xinjiang Medical University, Urumqi, P. R. China, 830011

[2] Department of Neurosurgery, The Second Affiliated Hospital of Xinjiang Medical University, Urumqi, P. R. China, 830063

*Corresponding author

Jianglong Yu

Address: Department of Neurosurgery, The Second Affiliated Hospital of Xinjiang Medical University,

Urumqi, 830028, P. R. China.

Email: yujianglong@xjmu.edu.cn

TEL：18199909986

Abstract

Background: Although temozolomide (TMZ) is a first-line chemotherapeutic agent for treating malignant gliomas, its mechanism of action remains to be incompletely understood, and elucidating the molecular mechanisms underlying TMZ's mode of action is crucial for improving its therapeutic efficacy.

Methods: This study aimed to delineate the effects of TMZ on glioma cells and the molecular mechanisms underlying its induction of ferroptosis. Using human glioma cell lines U87 and U251 as models, the impact of TMZ on cell proliferation, cell cycle, DNA integrity, and oxidative stress status were systematically evaluated through experiments including CCK-8, flow cytometry, and immunofluorescence. Further mechanistic investigations utilizing gene silencing and small molecule inducers were conducted to elucidate the pivotal role of glutathione peroxidase 4 (GPX4) in the ferroptosis process induced by TMZ.

Results: Results demonstrated that TMZ inhibited glioma cell proliferation, induced cell cycle arrest and DNA damage, while concurrently promoting reactive oxygen species (ROS) accumulation and glutathione (GSH) depletion, along with downregulation of GPX4 expression. Ferroptosis inducers Erastin or RSL3 significantly augmented TMZ's cytotoxicity, exacerbated lipid peroxidation and GSH consumption. GPX4 gene silencing also enhanced TMZ's cytotoxic effects and synergistically interacted with Erastin to promote ferroptosis. Furthermore, knockdown of ABCC1—a downstream target of GPX4—enhanced sensitivity to TMZ.

Conclusion: This study unveiled a novel mechanism that TMZ induced ferroptosis via the GPX4/ABCC1 pathway. These findings provided important insights into understanding molecular modes of action for TMZ, and offered insights into improving clinical therapeutic efficacy.

Keywords: Glioma, TMZ, GSH, GPX4, Ferroptosis, ROS

Introduction

Glioblastoma (GBM) stands out as the most aggressive primary malignant brain tumor, with a merely 3-5% of survival rate overall 5 years [1]. Despite the current standard treatment protocols, including surgical resection, radiation therapy, and adjuvant chemotherapy featuring temozolomide (TMZ), vast majority of patients eventually succumbed to tumor recurrence and drug resistance [2-3]. Hence, the exploration of effective novel therapeutic targets and strategies are of significance in enhancing the efficacy of GBM treatment.

In recent years, programmed cell death has emerged as a pivotal regulatory mechanism for tumor cell survival [4]. Alongside classical apoptosis, including several novel non-apoptotic forms of programmed cell death, such as ferroptosis, pyroptosis, and mitotic catastrophe, have garnered increasing attention [5]. These novel modes of cell demise exhibited unique biological characteristics and molecular mechanisms with their properties of distinct from apoptosis. Ferroptosis is a non-apoptotic form of programmed cell death induced by small molecules, such as the anti-tumor agent iron citrate [6]. Its primary biological features included the accumulation of free iron ions and reactive oxygen species (ROS) within cells, by which lipid peroxidation and ultimately resulting in cell membrane rupture, cellular swelling, and death were triggered [7-8]. Glutathione peroxidase 4 (GPX4) had been considered as one of the crucial negative regulators of ferroptosis, which capable of reducing and clearing intracellular lipid peroxides, thereby preventing ferroptosis [9-10]. It was illustrated that the antioxidant function of GPX4 relied on the supply of coenzymes, such as intracellular glutathione (GSH) [11].

Temozolomide (TMZ) is a frontline chemotherapy drug widely used clinically for GBM treatment. It exerts cytotoxic effects by inducing DNA damage and cell cycle arrest through DNA methylation [12]. H2AX is a variant of the H2A protein family and constitutes a component of the histone octamer in the nucleosome [13]. Previous studies proposed that in the PI3K pathway, H2AX was phosphorylated by kinases such as ataxia telangiectasia mutated (ATM) and ATM-Rad3-related (ATR) proteins [14]. Accordingly, investigations also illustrated that gamma H2AX served as the initial step in recruiting and localizing DNA repair proteins. Moreover, double-strand breaks (DSBs) could be induced by several mechanisms such as ionizing radiation or cytotoxic drugs, which led to the rapid formation of gamma-H2AX foci. These foci represented DSBs in a 1:1 ratio and could serve as biomarkers of damage [15-16]. However, clinical trails suggested that the efficacy of TMZ

typically diminished with prolonged treatment time, and closely associated with various mechanisms of resistance developed by tumor cells, such as enhanced DNA damage repair and dysregulation of cell cycle checkpoints [17-19]. Therefore, exploring novel anti-tumor mechanisms of TMZ and further combination with other strategies essential for improvements on its efficacy and reverse resistance.

The latest research had found that in glioblastoma, besides the traditional pathways of DNA damage and cell cycle arrest, TMZ might also induce ferroptosis to kill tumor cells [20-21]. TMZ could inhibit the expression of genes related to glutathione synthesis, by which decrease the GSH levels. In addition, TMZ also suppressed the expression and activity of GPX4, thereby disrupted the main defense pathway against ferroptosis [22]. Under conditions of GSH/GPX4 inhibition, TMZ might induce intracellular ROS and lipid peroxidation, further triggered ferroptosis and enhanced its cytotoxic effects [23]. Nevertheless, the mechanism of TMZ in inducing ferroptosis and further inhibit tumor growth remains to be unclear, and related studies are crucial and could provide valuable reference for GBM treatment.

In this study, human glioblastoma cell lines, U87 and U251, were utilized to investigate the novel mechanism of TMZ in inducing ferroptosis to inhibit tumor growth. The impact of TMZ on cell proliferation, cell cycle, DNA integrity and oxidative stress status through CKK-8, ROS imaging, GSH analysis, real-time fluorescence quantitative PCR analysis, western blot analysis, and further statistical analysis.

Materials and Methods

Cell Lines and Culture Conditions

Human U87 and U251 cell lines used in this study were purchased from Cellverse (Shanghai, China). The GBM cells were cultured in DMEM (Keycell, Wuhan, China) supplemented with 10% fetal bovine serum (ExCell Bio, Shanghai, China) and maintained in a humidified incubator at 37°C with 5% CO_2.

Reagents and Treatments

TMZ, Erastin, and RSL3 were purchased from Aladdin (Shanghai, China) and dissolved in DMSO to final concentrations of 50 mM, 1 mM, and 1 mM, respectively, for experimentation.

siRNA and Cell Transfection

GPX4 Smart silencer RNA (Ribobio, Guangzhou) and ABCC siRNA (Ribobio, Guangzhou) were synthesized and designed for cell transfection.

Cell Proliferation Assay

Cells were seeded at a density of 3×10^3 cells per well in a 96-well plate. Cells were treated with TMZ at final concentrations of 0, 50, 100, and 150 μM. Cell proliferation was assessed at 0, 24, 48, and 72 hours using the CCK-8 assay (Beyotime, Shanghai), following the manufacturer's instructions. Once the optimal TMZ concentration was determined, cells were seeded at a density of 3×10^3 cells per well in a 96-well plate, treated with TMZ at a final concentration of 150 μM, and supplemented with either Erastin (10 μM) or RSL3 (1 μM). Cell proliferation was then evaluated with the CCK-8 assay according to the manufacturer's instructions.

Cell Cycle Analysis

U87 and U251 cells in logarithmic growth phase with satisfactory growth status were seeded at a density of 3×10^5 cells per well in a 6-well cell culture plate, and incubated overnight at 37°C in a humidified atmosphere with 5% CO_2. After cells adhered completely, they were treated with 150 μM TMZ for 48 hours. Cells were then collected by trypsin digestion, centrifuged at 1200 rpm for 5 minutes, and the supernatant was removed. Cells were washed twice with PBS and resuspended in 100 μl of PBS. Slowly, 700 μl of pre-cooled 80% ethanol was added to achieve a final concentration of 70% ethanol. Cells were fixed at 4°C for 4 hours followed by centrifugation at 1500 rpm for 5 minutes. After washing twice with pre-cooled PBS, cells were resuspended in 200 μl of PBS. Subsequently, 10 μl of 1 mg/ml RNase (Sigma-Aldrich, USA) was added, and cells were

incubated at 37°C for 30 minutes. Then, 10 µl of 400 µg/ml propidium iodide (PI) (Sigma-Aldrich, USA) was added, and cells were stained in the dark at 4°C for 30 minutes. Ultimately, cell cycle analysis was performed using a flow cytometer.

Immunofluorescence

U87 and U251 cells were seeded onto glass slides and treated with 150 µM TMZ for 48 hours. After incubation, cells were fixed with 2% paraformaldehyde at room temperature for 5 minutes, and washed three times with PBS, permeabilized with 0.2% PBS-Triton X-100 for 4 minutes, then incubated in 3% PBS-BSA for 30 minutes to minimize non-specific binding. Subsequently, the fixed cells were incubated with rabbit anti-phospho-gamma-H2AX (S139) antibody (Abcam, UK) for 1 hour, washed three times with 3% PBS-BSA, then incubated with Cy3-conjugated anti-rabbit secondary antibody (BOSTER, Wuhan, China) for 45 minutes. After incubation, cells were washed three times with PBS and mounted with glycerol-PBS medium containing 50 mg/ml DABCO. As a final step, imaging was performed using an Olympus BX53 fluorescence microscope (Olympus, Japan).

ROS Imaging

Cells were seeded onto 6-well chamber slides (5×10^5 cells per well) and incubated for 24 hours. After washing the chamber slides with PBS, they were incubated with BDP 581/591 C11 (Dojindo, Japan) or DCFH-DA (Beyotime, Shanghai) working solution for 30 minutes. Subsequently, imaging was performed using a BX53 fluorescence microscope (Olympus, Japan).

GSH Analysis

GSH detection was performed using a GSH assay kit (Solarbio, Beijing), following the manufacturer's instructions for GSH determination.

Real-Time Fluorescence Quantitative PCR Analysis

Total RNA extracted from U87 and U251 cells was subjected to two-step real-time reverse transcription-polymerase chain reaction (RT-PCR). Cells were collected and lysed, and total RNA was extracted using TRIzol reagent (Thermo Fisher Scientific, USA). cDNA synthesis was performed using reverse transcription reagents (Vazyme, Nanjing), followed by real-time RT-PCR analysis. The primer sequences were as follows:

GAPDH-F: 5′-TCAAGAAGGTGGTGAAGCAGG-3′,

GAPDH-R: 5′- TCAAAGGTGGAGGAGTGGGT-3′;

GPX4-F: 5′-ATACGCTGAGTGTGGTTTGC-3′,

GPX4-R: 5′-CTTCATCCACTTCCACAGCG-3′;

SLC7A11-F: 5′-TGTGTGGGGTCCTGTCACTA-3′,

SLC7A11-R: 5′-GCAGGGCGTATTATGAGGAG-3′;

HMOX1-F: 5′-TCTTTGAGGAGTTGCAGGAGC-3′,

HMOX1-R: 5′-AGTGTAAGGACCCATCGGAGAA-3′;

ABCC1-F: 5′-ATGACACCTCTCAACAAAACCAAAA-3′,

ABCC1-R: 5′-ATGATCCCTGAAGACTGAACTC-3′.

All templates were initially denatured at 95°C for 10 minutes, followed by 40 cycles of denaturation at 95°C for 10 seconds, annealing at 60°C for 60 seconds, and extension at 72°C for 30 seconds. Real-time RT-PCR analysis was performed using PCR reaction mixtures contained with SYBR GREEN dye (TOLOBIO, Shanghai) to evaluate mRNA expression. PCR amplification was carried out using the ViiA™ 7 Real-Time PCR System (Thermo Fisher Scientific, USA).

Western Blot Analysis

After cell lysis, protein was extracted and quantified using a BCA protein assay kit (GBCBIO, Guangzhou). Subsequently, proteins were separated by SDS-PAGE and transferred onto nitrocellulose membranes (Millipore, USA). The membranes were blocked in PBS containing 5% (w/v) skim milk powder for 1 hour, followed by overnight incubation at 4°C with primary antibodies, including anti-GAPDH (1:1000) (Goodhere, Hangzhou), anti-GPX4 (1:1000) (BIOSS, Beijing), and anti-ABCC1 (1:1000) (BIOSS, Beijing). The membranes were then incubated with corresponding HRP-conjugated secondary antibodies (Beyotome, Shanghai), and then visualized using chemiluminescent substrates (Servicebio, Wuhan).

Statistical Analysis

Statistical analysis was performed using GraphPad Prism 5 (GraphPad Software Inc., USA). All in vitro experimental results were expressed as the mean ± standard deviation (mean ± SD) of at least three independent experiments. Each graph represents independent data points from each experiment. Statistical significance between different datasets was compared using unpaired two-tailed Student's t-test or two-way ANOVA (when comparing more than two groups), followed by Bonferroni post hoc test (*$p < 0.05$, **$p < 0.01$, ***$p < 0.001$). For database analysis, $p < 0.05$ was considered statistically significant.

Results

Temozolomide (TMZ) inhibits the proliferation of glioma cells and induces oxidative stress-related effects.

Cell viability was assessed using the CCK-8 assay to determine the impact of different concentrations of TMZ at different time points on the growth of glioma cells. In 24 h, the 150 μM condition take a slightly lower value compared with other conditions, and the higher the concentration, the lower the OD value. Accordingly, the OD values were continuously decreased and the group differences were more obvious during 72 hours, where the 150 μM condition had the lowest value and 0 μM concentration owned the highest OD value. The results showed that TMZ exhibited dose-and time-dependent inhibitory effects on glioma cells U87 and U251 (Supplementary Figure 1 A and B). Further investigation using flow cytometry to examine the cell cycle revealed that treatment with 150 μM TMZ for 48 hours led to G0/G1 phase arrest in U87 cells and G2/M phase arrest in both U87 and U251 cells (Supplementary Figure 2 A and B).

Immunofluorescence results showed that TMZ also promoted the occurrence of DNA double-strand breaks (Supplementary Figure 3). At the molecular level, TMZ not only induced the generation of reactive oxygen species (ROS) (Supplementary Figure 4) but also inhibited the production of the antioxidant glutathione (GSH) (Supplementary Figure 5). ROS served as an indicator of oxidative stress, while GSH acted as a factor inhibiting ROS, indicated that TMZ could induce oxidative stress and disrupt the cellular redox balance. These foundational data lay the groundwork for further exploration of the molecular mechanisms underlying TMZ-induced ferroptosis.

TMZ Inhibits GPX4 Expression

As shown in figure 1, Following treatment with 150 μM TMZ, both U87 and U251 cell lines exhibited a significant decrease in GPX4 expression at RNA levels, and the trend was more obvious in U251 cell lines (Figure 1 A and 1B). Moreover, same notable decrease in GPX4 expressions were observed at protein level, and the trend were more pronounced in U251 cell lines (Figure 1C and 1D).

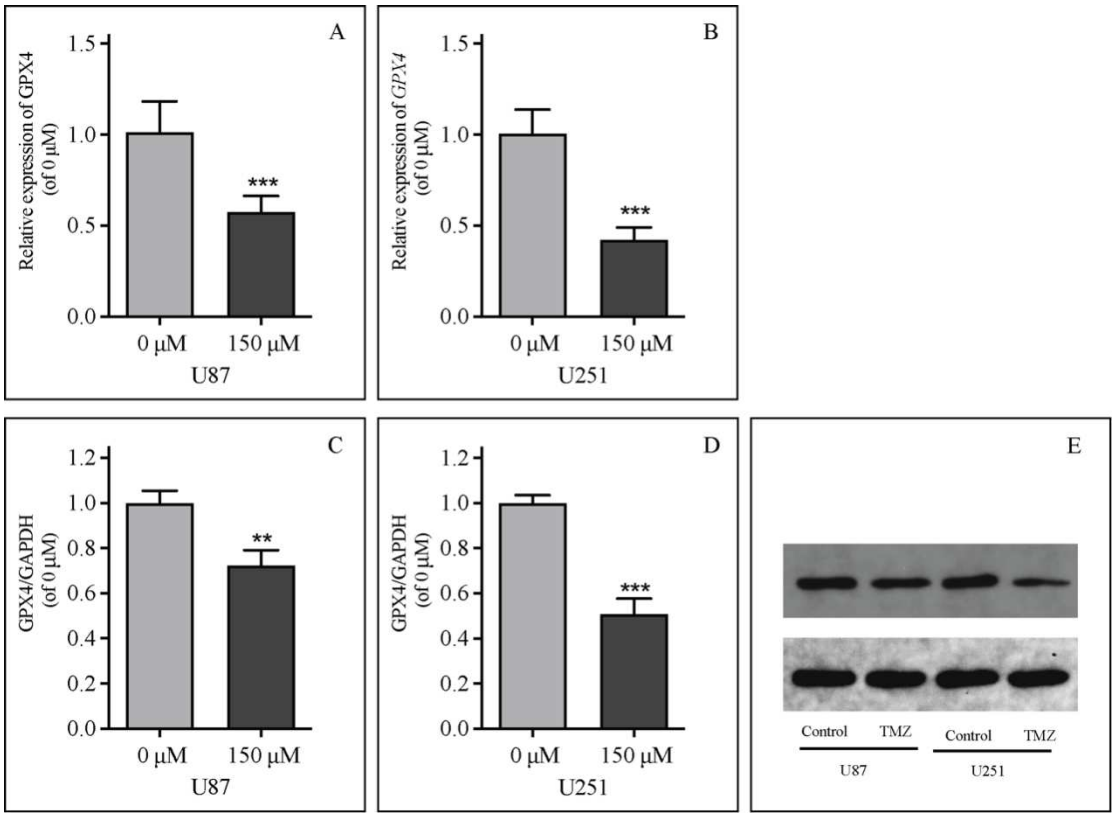


Figure 1. TMZ Inhibits GPX4 Expression in Glioblastoma Cells

qPCR Data Analysis: U87 Cells (A); U251 Cells (B)

Western Blot Analysis: U87 Cells (C); U251 Cells (D)

TMZ Suppresses Glioblastoma Cells via Promoting Ferroptosis

Ferroptosis inducers significantly inhibit cell proliferation under TMZ treatment.

Figure 2 illustrated the results of glioblastoma cell viability under the combination of TMZ and ferroptosis inducers. In U87 and U251 cells, the OD value was highest in control group, and the value were lower in TMZ and Erastin groups. Noticeably, the combination of TMZ+Erastin were decreased the OD value more obviously. Same decreasing trend were observed in RSL3 group, and the reducing trend were more significant in the TMZ+RSL3 group. Accordingly, upon treatment with 150 μM TMZ in glioblastoma cell lines U87 and U251, the addition of Erastin (10 μM) or RSL3 (1 μM) significantly inhibited cell proliferation (Figure 2 A and B).

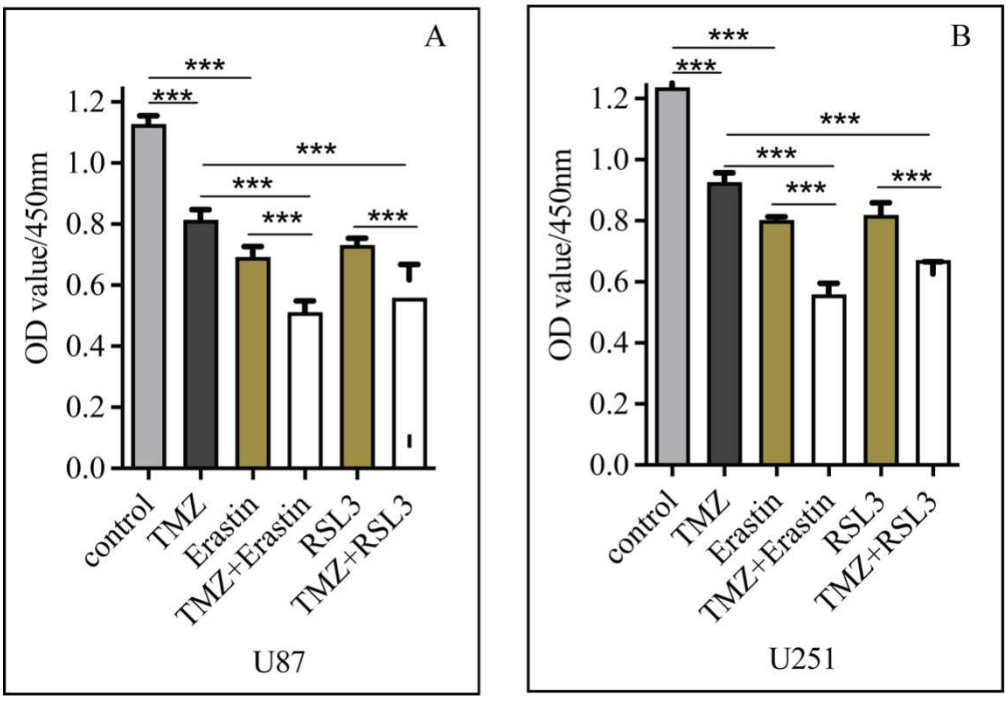


Figure 2. Combination of TMZ and Ferroptosis Inducers Significantly Suppresses Glioblastoma Cell Viability

The result of reversal of the combined effect of TMZ and ferroptosis inducers on U87 and U251 cells treated with ferrostain-1 were provided in figure 3. The OD values were diminished at certain level in the TMZ, Erastin, RSL3, TMZ+Erastin, and TMZ+RSL3 groups, and, however, a markedly increasing trend were observed in TMZ+Erastin+ferrostain-1, and TMZ+RSL3+ferrostain-1 groups. These results suggested that the reduction in cell viability was reversed by the ferroptosis inhibitor Ferrostatin-1 (Figure 3 A and B).

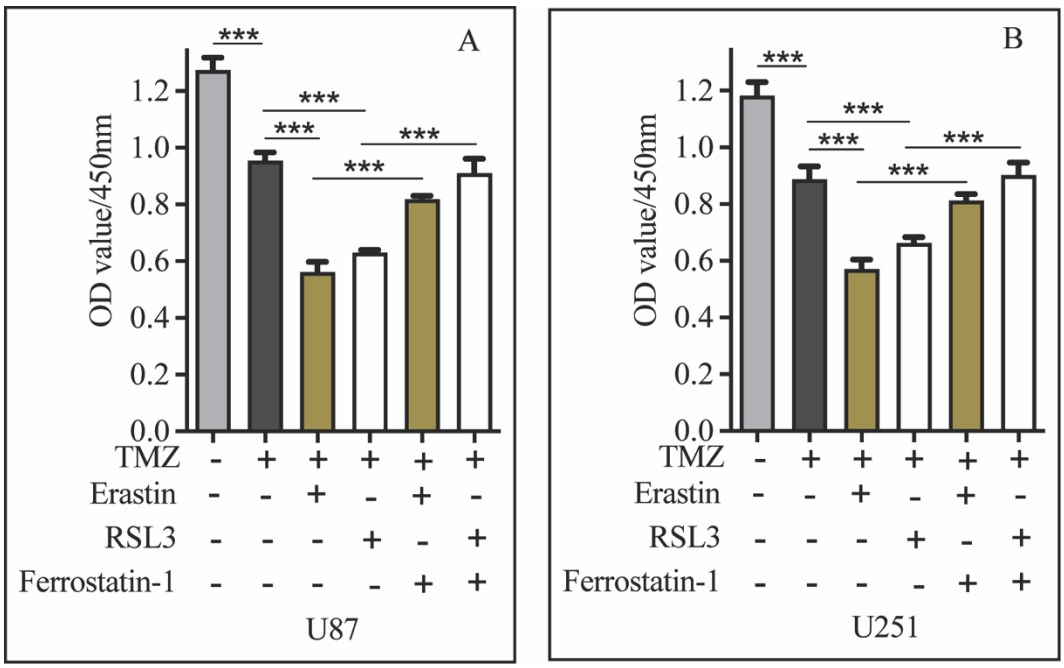


Figure 3. Reversal of the Combined Effect of TMZ and Ferroptosis Inducers by Ferrostatin-1

Ferroptosis inducers significantly promote lipid peroxidation and inhibit GSH under TMZ treatment.

The lipid peroxidation probe BDP 581/591 C11 is a fluorescent dye used to detect the formation of lipid peroxides. This fluorescent dye does not react with lipid peroxides but reacts with lipid radicals formed during the highly sensitive oxidation process by reactive oxygen species. Upon treatment with 150 μM TMZ in glioblastoma cell lines U87 and U251, the addition of Erastin (10 μM) or RSL3 (1 μM) significantly promotes lipid peroxidation (Figures 4 and 5). The analysis of GSH levels demonstrates that the combination of TMZ and ferroptosis inducers Erastin (10 μM) or RSL3 (1 μM) significantly promotes lipid peroxidation (Figure 6). GSH values showed a decreasing trend in TMZ, Eeastin and TMZ+Erastin groups in U87 and U 251 cell lines, and lest group (TMZ+Erastin) showed the lowest value. RSL3 and TMZ+RSL3 groups also showed lower GSH values compared to the control group, and the combined group had owned the most significant decrease among these two groups. The analysis of GSH levels demonstrates that the combination of TMZ and ferroptosis inducers Erastin (10 μM) or RSL3 (1 μM) significantly promotes lipid peroxidation (Figure 6 A and B).

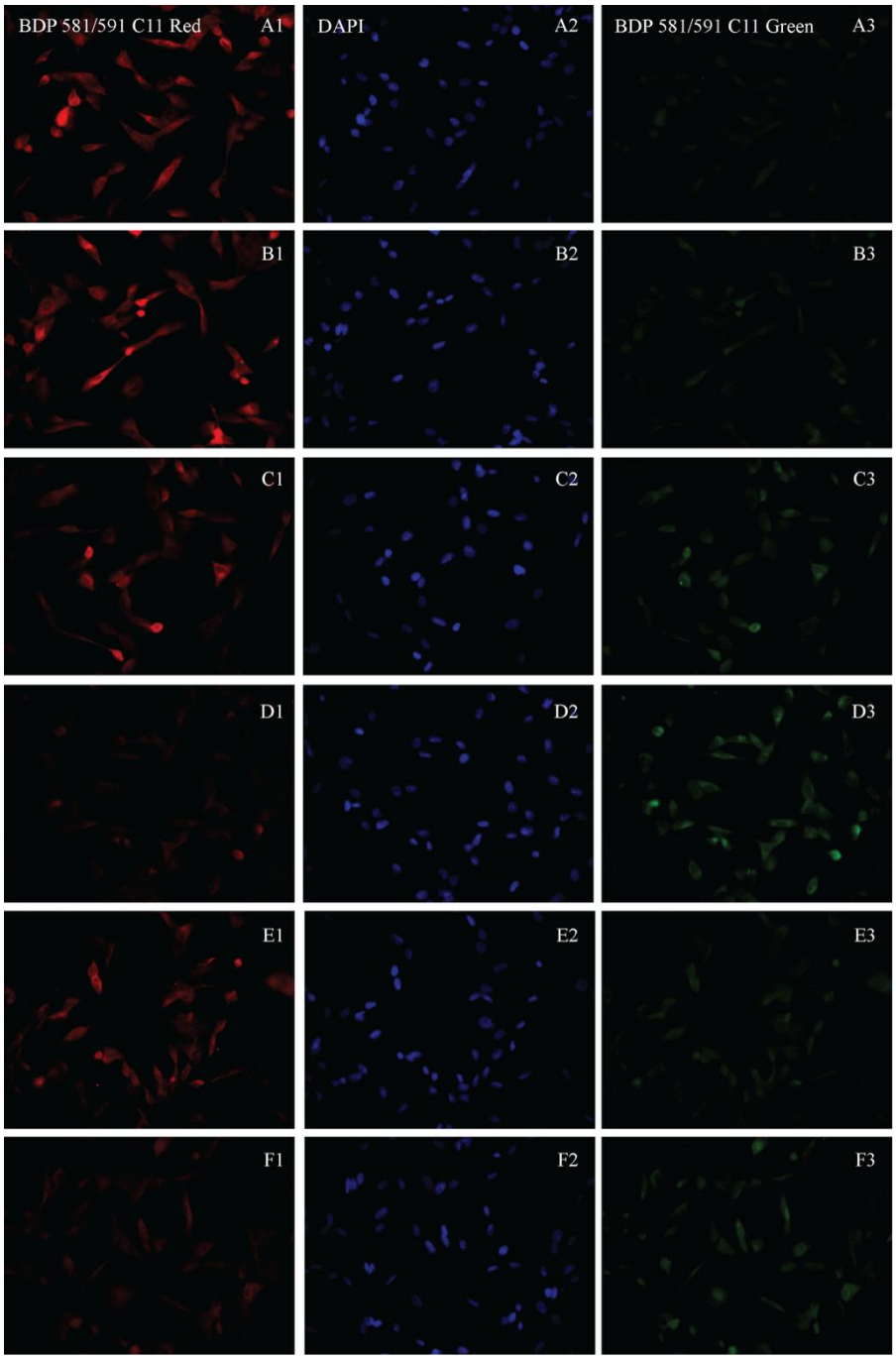


Figure 4. Ferroptosis Inducers Enhance TMZ-Mediated Lipid Peroxidation in Glioblastoma Cells (U87); A: U87 normal cells; B: U87 cells treated with TMZ (150 μM) for 48h; C: U87 cells treated with Erastin (10 μM) for 48h; D: U87 cells treated with TMZ (150 μM) and Erastin (10 μM) for 48h; E: U87 cells treated with RSL3 (1 μM) for 48h; F: U87 cells treated with TMZ (150 μM) and RSL3 (1 μM) for 48h.

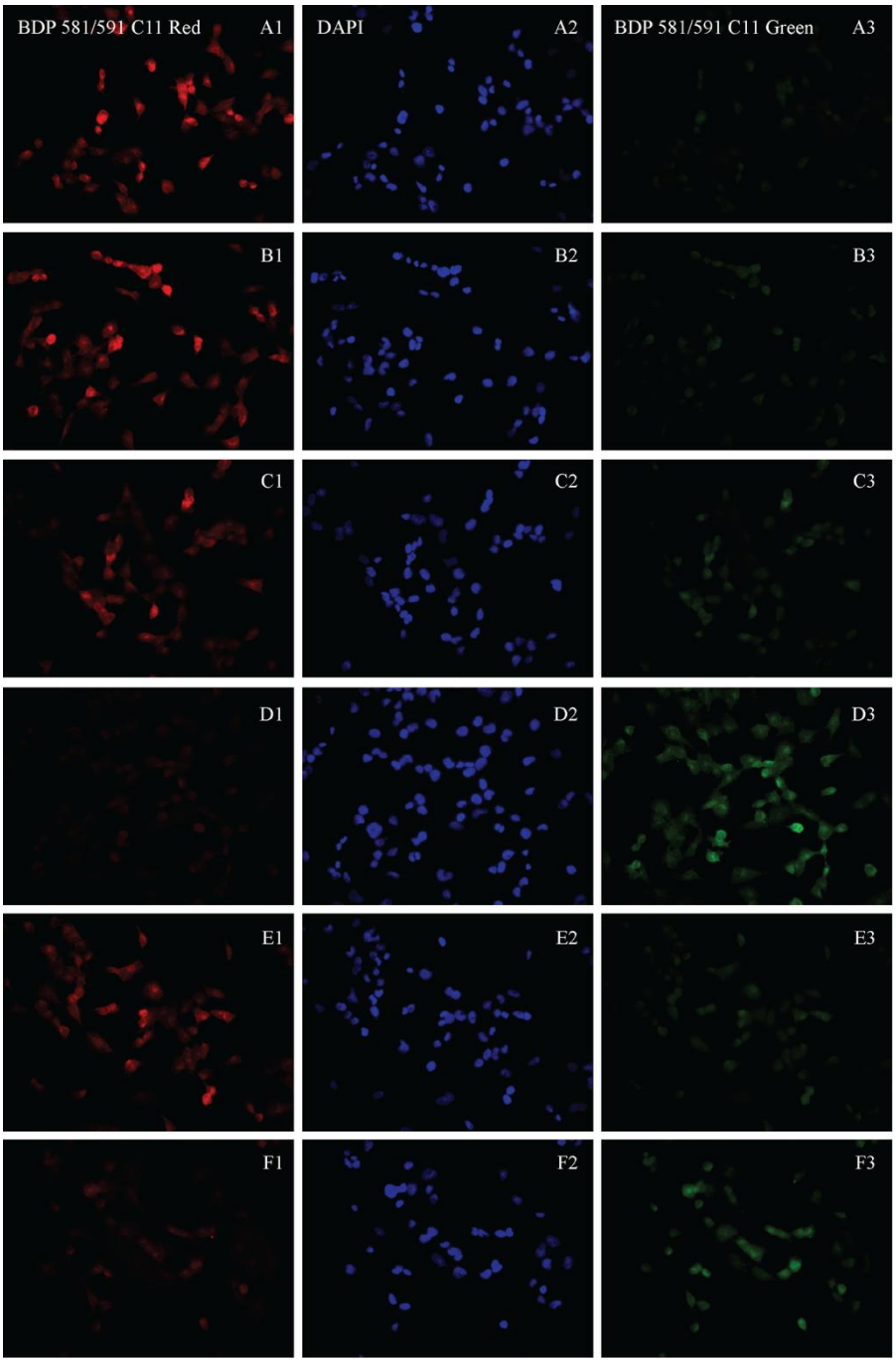


Figure 5. Ferroptosis Inducers Enhance TMZ-Mediated Lipid Peroxidation in Glioblastoma Cells (U251); A: U251 normal cells; B: U251 cells treated with TMZ (150 μM) for 48h; C: U251 cells treated with Erastin (10 μM) for 48h; D: U251 cells treated with TMZ (150 μM) and Erastin (10 μM) for 48h; E: U251 cells treated with RSL3 (1 μM) for 48h; F: U251 cells treated with TMZ (150 μM) and RSL3 (1 μM) for 48h.

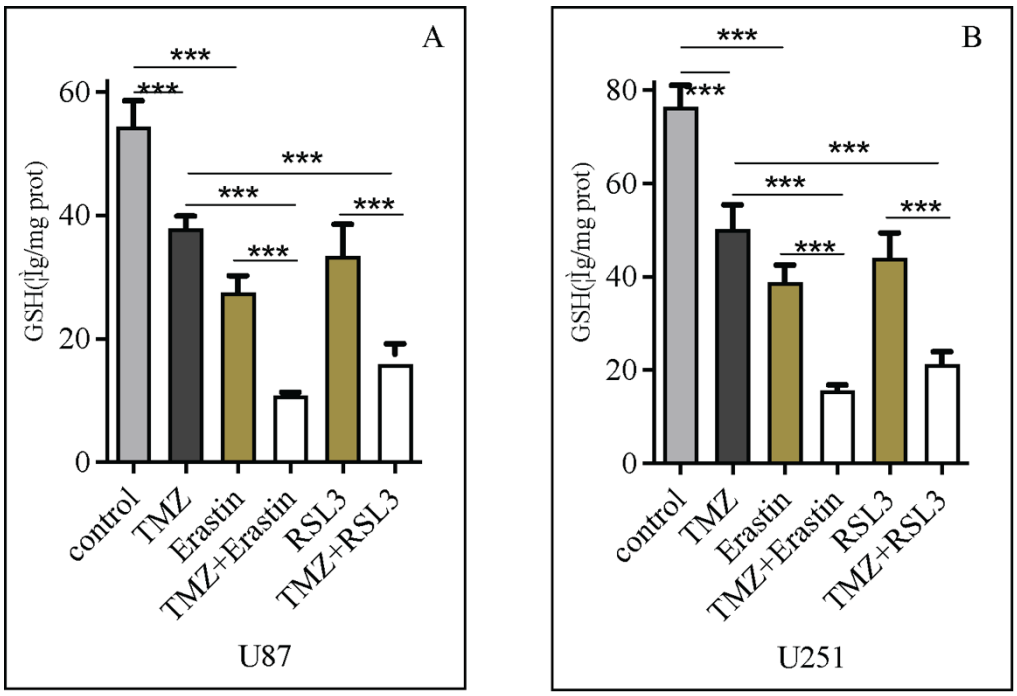


Figure 6. Combination of TMZ and Ferroptosis Inducers Significantly Inhibits GSH Levels in Glioblastoma Cells

Silencing of GPX4 Promotes Ferroptosis Through GSH Regulation

Regulation of Downstream Gene Expression by GPX4 Silencing

Glioblastoma cell lines U87 or U251 were transfected with GPX4 smart silencer RNA (siGPX4), subsequently, qPCR and Western blot were conducted to verify the silencing effect. Results showed that, in above cell lines, compared to the control group (siNC), the relative expression of SLC7A11 and ABCC1 were noticeably downregulated in GPX4 mRNA (Figure 7 A, B, D, E, F, and H), while the relative expression of HMOXI were remarkably upregulated (Figure 7 C and G). In the protein, same trend were observed, the GPX4/GAPDH and ABCC1/GAPDH were significantly downregulated in the siGPX4 group compared to the control (siNC) group (Figure 8 B-E). Further analysis of downstream genes of GPX4 revealed that SLC7A11 and ABCC1 were downregulated while HMOX1 was upregulated, which demonstrated by qPCR (Figure 7 C and G), and consistent with Western blot results (Figure 8 A).

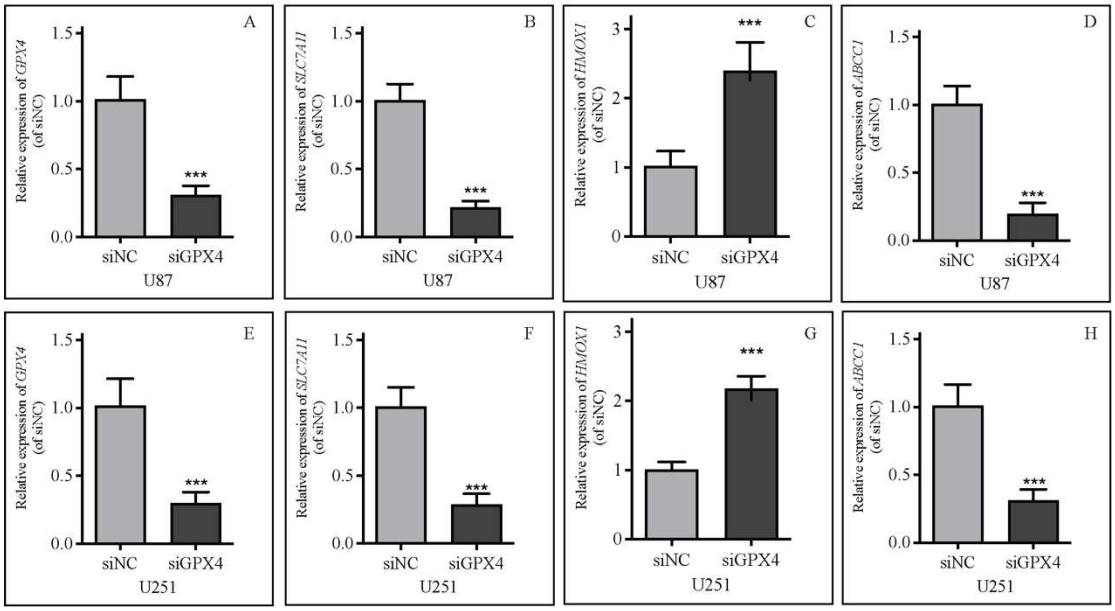


Figure 7: qPCR Quantitative Analysis of Downstream Target Gene Expression Regulated by GPX4

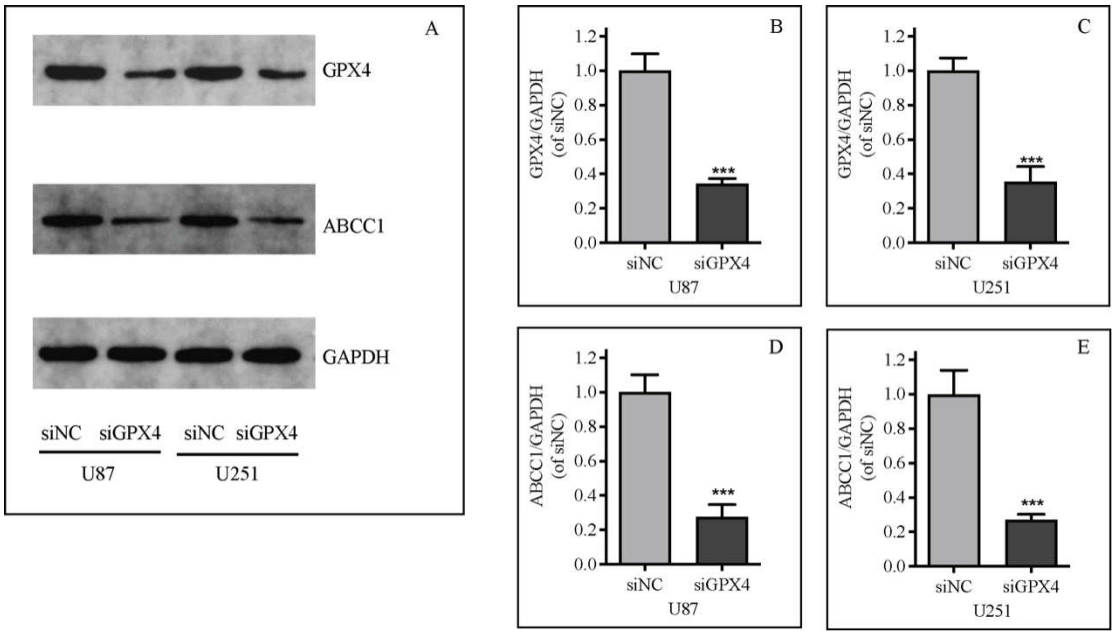
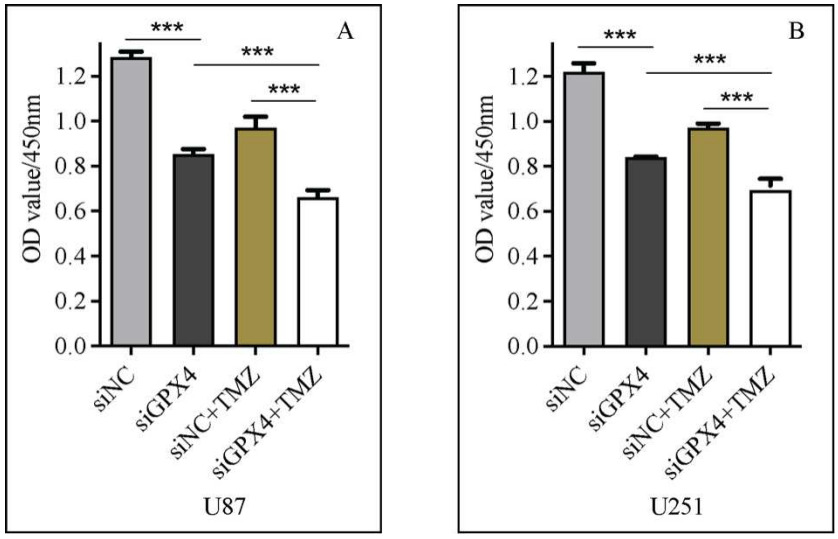


Figure 8: Western Blot Analysis of GPX4 Impact on ABCC1 Expression

Silencing GPX4 Potentiates the Inhibitory Effect of TMZ on Glioblastoma Cell Viability

As shown in figure 9, based on the CCK-8 analysis, the OD values of siGPX4, siNC+TMZ, siGPX4+TMZ groups were significantly lower than that of siNC group in both U87 and U51 cell lines (Figure 9 A and B). Among the groups, the siNC group had relatively higher OD value compared to siGPX4 and siGPX4+TMZ groups, and the siGPX4+TMZ group had showed the lowest value, these results illustrated that, upon treatment with 150 μM TMZ, silencing GPX4

195 significantly suppressed the viability of glioblastoma cells treated with TMZ.



196

197 Figure 9: Silencing GPX4 Significantly Inhibits the Viability of Glioblastoma Cells Treated

198 with TMZ

199 **Silencing GPX4 Combined with Erastin Inhibits the Viability of Glioblastoma Cells**

200 The results of the effect of Silencing GPX4 Combined with Erastin on U87 and U251 cell lines

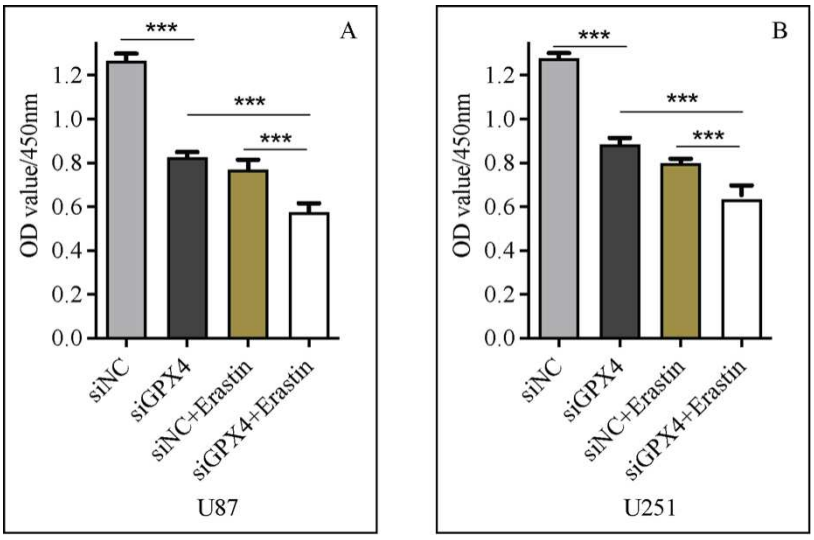
201 were revealed in figure 10. The OD values of siGPX4, siNC+Erastin, siGPX4+Erastin groups were

202 significantly lower than that of siNC group(Figure 10 A and B). The siGPX4+Erastin group had the

203 lowest OD value, and the siNC+Erastin group had a slightly lower value compared to siGPX4 group.

204 Building upon Erastin's inhibition of glioblastoma cell viability, silencing GPX4 further

205 significantly suppresses the cell viability of both U87 and U251 glioblastoma cells.



206

207 Figure 10. Silencing GPX4 Significantly Inhibits the Viability of Glioblastoma Cells in the

208 Presence of Erastin

Silencing GPX4 and Erastin Combined Treatment Promotes Oxidative Stress Damage in Glioblastoma Cells

As depicted in figure 11, the GSH levels were remarkably suppressed in siGPX4, siNC+Erastin, siGPX4+Erastin groups in both U87 and U251 cell lines. In which, the GSH were most effectively suppressed in siGPX4+Erastin group, and the GSH level of siGPX4+Erastin group was relatively lower than that of siGPX4 group (Figure 11 A and B). Building upon this, silencing GPX4 further significantly suppressed cellular GSH levels in U87 and U251 glioblastoma cells treated with Erastin (Figure 11). The combined action of silencing GPX4 and Erastin led to increased ROS production (Figure 12) and DNA damage (Figure 13) in glioblastoma cells.

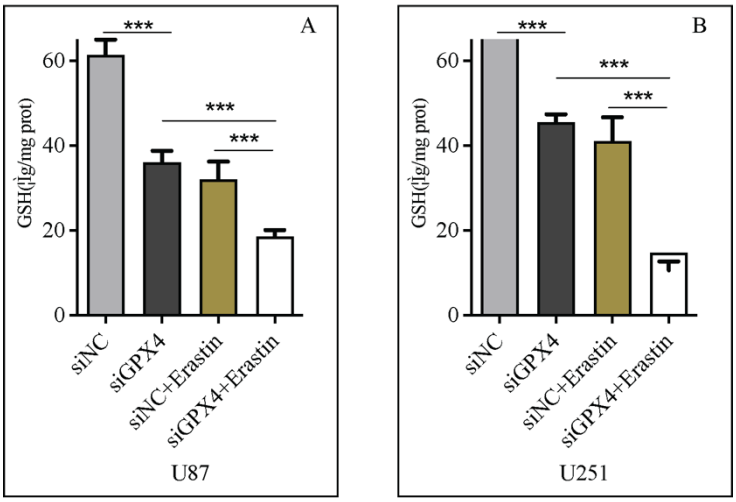


Figure 11. Silencing GPX4 Significantly Inhibits GSH Levels in Glioblastoma Cells Under Erastin Treatment

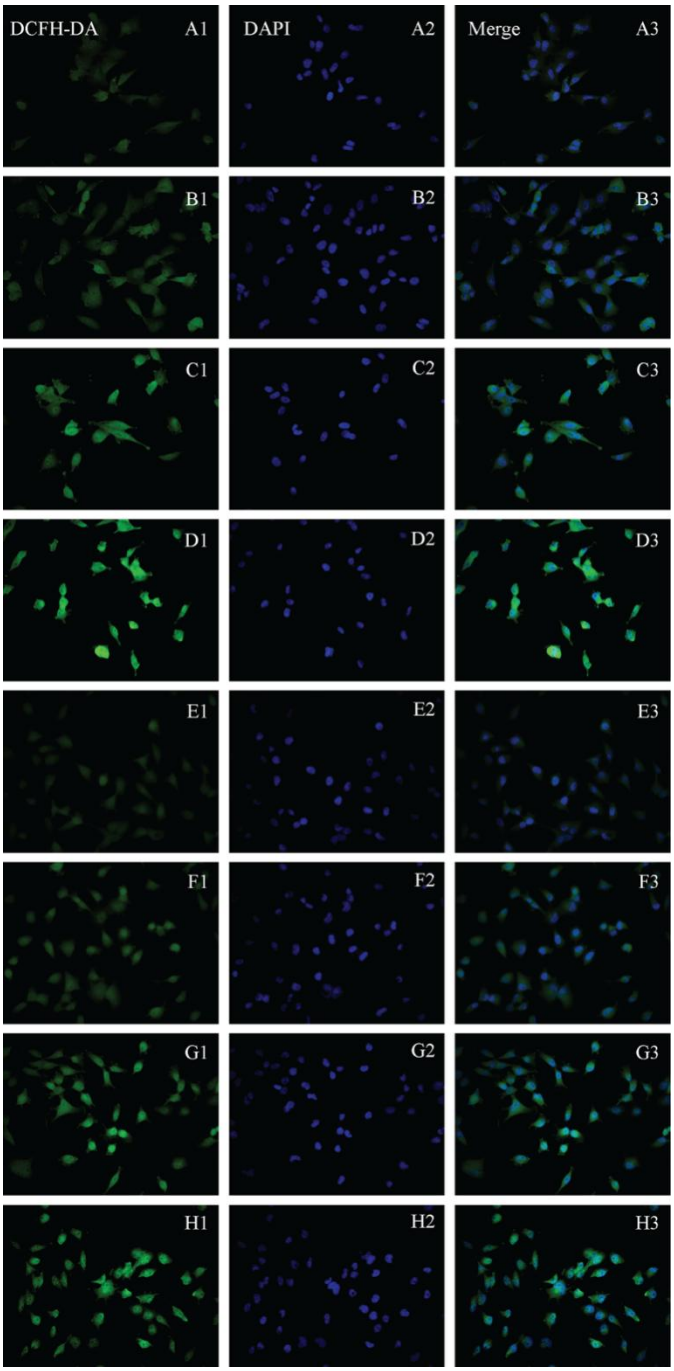


Figure 12. Silencing GPX4 Significantly Increases ROS Levels in Glioblastoma Cells Under Erastin Treatment; U87 cells (A: siNC; B: siGPX4; C: siNC + Erastin; D: siGPX4 + Erastin); U251 cells (E: siNC; F: siGPX4; G: siNC + Erastin; H: siGPX4 + Erastin);

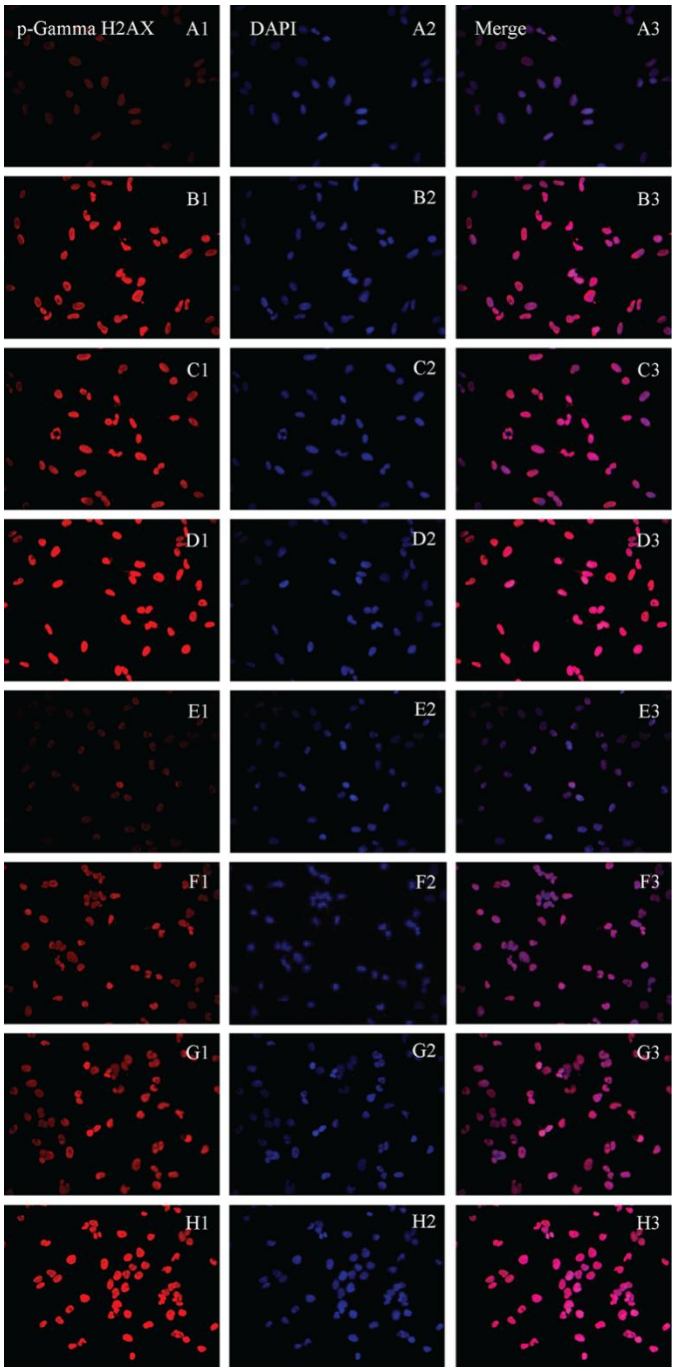


Figure 13 Silencing GPX4 Significantly Increases DNA Damage in Glioblastoma Cells Under Erastin Treatment; U87 cells (A: siNC; B: siGPX4; C: siNC + Erastin; D: siGPX4 + Erastin); U251 cells (E: siNC; F: siGPX4; G: siNC + Erastin; H: siGPX4 + Erastin);

Silencing GPX4 and ABCC1 Significantly Inhibits Glioblastoma Cell Viability

The previous results indicated that silencing GPX4 is associated with the inhibition of tumor cell viability, and GPX4 regulates the expression of ABCC1. Therefore, we hypothesized that simultaneous inhibition of GPX4 and ABCC1 would significantly suppress glioblastoma cell viability. The inhibiting efficiency results of Silencing GPX4 and ABCC1on Glioblastoma Cell

Viability were illustrated in figure 14. The OD values of siGPX4, siABCC1, and siGPX4+siABCC1 groups were remarkably lower than that of siNC group, in which the siGPX4+siABCC1 group had the smallest value compared with others. Noticeably, the siABCC1 group owned a close yet relatively lower value versus siGPX4 group in U87 group, while the difference between siABCC1 and siGPX4 groups were more obvious in U251 cell lines. Above experimental results are consistent with our expectations (Figure 14).

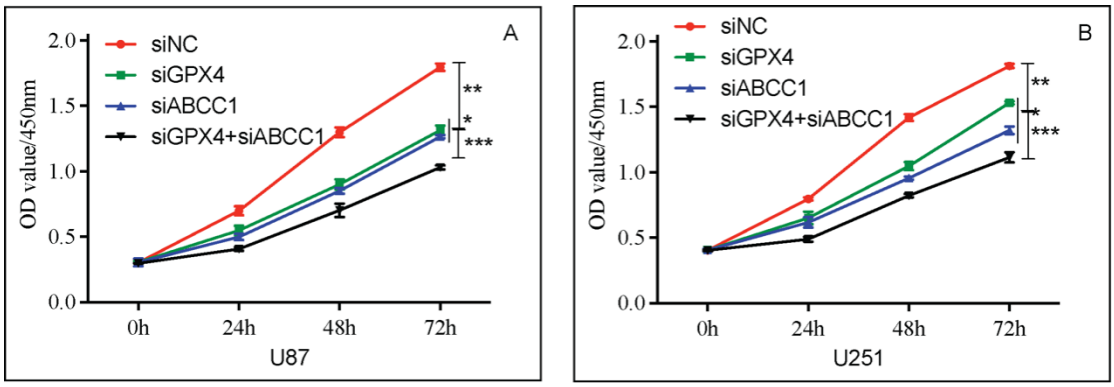


Figure 14: Silencing GPX4 and ABCC1 Significantly Inhibits Glioblastoma Cell Viability

Discussion

This study unveiled a novel mechanism that TMZ inhibits glioblastoma cell proliferation through inducing ferroptosis. Our findings demonstrated that TMZ not only triggers DNA damage and cell cycle arrest, and elevated intracellular ROS levels, but also reduces GSH levels, suppresses GPX4 expression, and disrupting the delicate balance of GSH/GPX4-mediated defense against ferroptosis. These alterations created a conducive environment for TMZ-induced ferroptosis in tumor cells. Viswanathan et al. [24] elucidated that TMZ induced ferroptosis-dependent therapy resistance in breast cancer and non-small cell lung cancer cells by impeding GSH synthesis and GPX4 activity, thereby fostering ferroptosis. Similarly, Yang et al. [25] underscored GPX4 as a pivotal regulator in cellular defense against ferroptosis, where its antioxidative role hinged on GSH supply. Furthermore, they found that various anticancer agents, including TMZ and Erastin, provoke ferroptosis by targeting GPX4. Moreover, our extended investigations revealed that concurrent treatment with ferroptosis inducers like Erastin or RSL3 significantly potentiated TMZ's cytotoxicity against glioblastoma cells, suggesting that ferroptosis mediated a substantial portion of TMZ's cytotoxic effects. This observation mirrored the findings of Dixon et al. [26], who

demonstrated that ferroptosis inducers like Erastin and RSL3 inhibit GSH synthesis by targeting system Xc-, culminating in ferroptosis induction.

These findings collectively support the notion that TMZ could induce cell death in tumor cells through the ferroptosis pathway. However, present work further elucidated the molecular regulatory network underlying TMZ-induced ferroptosis, including ROS, GSH, GPX4, and their downstream genes. This provided novel biomarkers and potential therapeutic targets for targeted interventions in ferroptosis.

SLC7A11 is a system transporter closely involved in cystine uptake and GSH synthesis, whereas ABCC1 is an ATP-binding cassette transporter involved in GSH efflux. Interestingly, results of our work illustrated that silencing GPX4 not only directly induced ferroptosis but also downregulated the expression of SLC7A11 and ABCC1. These findings were in line with the published work of Xu T et al. [27], where they demonstrated GPX4's crucial role as an anti-ferroptotic protein and its downregulation leading to lipid peroxidation accumulation and ferroptosis. Moreover, they found that GPX4 modulated GSH levels by regulating the expression of cystine transporter SLC7A11 and GSH synthesis-related genes. These results suggest that GPX4 might regulate ferroptosis by modulating the synthesis and metabolism of GSH, elucidating the central rule of GPX4's in ferroptosis. Additionally, elevations in HMOX1 expression were observed in both U87 and U251 cells, encoding heme oxygenase that promotes iron release, and further facilitating ferroptosis. This observation corroborated with the published work of Cao JY et al. [28], where they demonstrated that overexpression of heme oxygenase 1 (HMOX1) promoted iron ion release and exacerbated lipid peroxidation, thereby inducing ferroptosis in tumor cells. Above results unveiled multiple regulatory mechanisms of GPX4 in the ferroptosis pathway.

Ferroptosis is a form of cell death regulated by both iron ions and lipid peroxidation. In this study, our findings directly confirmed the significant promotion of lipid peroxidation and ROS production by TMZ in combination with ferroptosis inducers, as evidenced by the fluorescence levels of BDP581/591 C11 and DCFH-DA. This phenomenon was closely associated with the decrease in GSH levels. GSH, as one of the major antioxidants in the body, plays a crucial buffering and defensive role during ferroptosis. Therefore, our outcomes suggested that TMZ/ferroptosis inducers inhibited GSH synthesis, further disrupted the cellular defense mechanisms against ferroptosis, led to exacerbated oxidative stress and lipid peroxidation, ultimately triggered

ferroptosis. Forcina GC et al. [29] found that inhibiting GSH synthesis or blocking the GSH transporter ABCC1 could promote ferroptosis in tumor cells, highlighting the critical role of GSH in ferroptotic defense. Above findings supported our observation of decreased GSH levels with TMZ/ferroptosis inducers. Additionally, Gao M et al. [30] reported that besides inducing gene damage through DNA methylation, TMZ could also increase intracellular ROS levels and lipid peroxidation, suggesting its potential to induce ferroptosis. Our present study results were also consistent with the previous finding and their conclusions.

In summary, this study elucidated the molecular mechanism of TMZ-induced ferroptosis in glioblastoma cells, and unveiled a novel mechanism that TMZ induces ferroptosis via the GPX4/ABCC1 pathway, which hopefully provided new insights into the novel anti-tumor effect of TMZ. By investigating the relationship between TMZ and ferroptosis, this study not only deepened the understanding of the pharmacological effects of TMZ but also provided new insights into its therapeutic efficacy via combination with other ferroptosis modulators in the future. It is worth noting that this study primarily focuses on in vitro cellular levels, and thus, further validations in animal models and clinical samples is needed to assess its feasibility and safety for in vivo and clinical applications. Additionally, due to the involvement of complex upstream and downstream regulatory networks in the process of ferroptosis, further research on other related molecules and signaling pathways are warranted to comprehensively elucidate the landscape of TMZ-induced ferroptosis.

Abbreviations

TMZ	Temozolomide
GPX4	glutathione peroxidase
ROS	oxygen species
GSH	glutathione
GBM	Glioblastoma
ATM	ataxia telangiectasia mutated
ATR	ATM-Rad3-related
DSBs	double-strand breaks
RT-PCR	reverse transcription-polymerase chain reaction
HMOX1	heme oxygenase 1

Statements and Declarations

Ethics approval and consent to participate

Not applicable. This study did not involve human or animal experiments.

Consent for publication

Not applicable.

Data Availability Statement

The datasets generated during analyzed the current study are available from the corresponding author on reasonable request.

Competing interests

The authors declare no competing interests.

Funding

This work was financially supported by State Key Laboratory of Pathogenesis, Prevention and Treatment of High Incidence Diseases in Central Asia, Xinjiang Medical University: State Key Laboratory of Pathogenesis, Prevention and Treatment of High Incidence Diseases in Central Asia Fund (Project No: SKL-HIDCA-2022-JZ9), and Xinjiang Key Laboratory of Neurological Disorder Research (Project No:XJDX1711-2224).

Authorship contribution statement

Jianglong Yu: Conceptualization, Methodology, Investigation, Writing–original draft, Project administration，Funding acquisition; Abudula·Aisha: Visualization，Writing–review & editing; Yan Yang and Xinping Luan: Visualization, Writing–review & editing; Xu Zhang and Yongji Zhu: Methodology, Investigation.

Acknowledgments

The authors are grateful for the reviewer’s valuable comments that improved the manuscript.

References

[1]. Omuro A, DeAngelis LM. Glioblastoma and other malignant gliomas: a clinical review. JAMA. 2013 Nov 6;310(17):1842-50. doi: 10.1001/jama.2013.280319. PMID: 24193082.

[2]. Yang K, Wu Z, Zhang H, et al. Glioma targeted therapy: insight into future of molecular approaches. Mol Cancer. 2022 Feb 8;21(1):39. doi: 10.1186/s12943-022-01513-z. PMID: 35135556; PMCID: PMC8822752.

[3]. McBain C, Lawrie TA, Rogozińska E, et al. Treatment options for progression or recurrence of glioblastoma: a network meta-analysis. Cochrane Database Syst Rev. 2021 May 4;5(1):CD013579. doi: 10.1002/14651858.CD013579.pub2. PMID: 34559423; PMCID: PMC8121043.

[4]. Galluzzi L, Vitale I, Aaronson SA, et al. Molecular mechanisms of cell death: recommendations of the Nomenclature Committee on Cell Death 2018. Cell Death Differ. 2018 Mar;25(3):486-541. doi: 10.1038/s41418-017-0012-4. Epub 2018 Jan 23. PMID: 29362479; PMCID: PMC5864239.

[5]. Conrad M, Angeli JP, Vandenabeele P, et al. Regulated necrosis: disease relevance and therapeutic opportunities. Nat Rev Drug Discov. 2016 May;15(5):348-66. doi: 10.1038/nrd.2015.6. Epub 2016 Jan 18. PMID: 26775689; PMCID: PMC6531857.

[6]. Stockwell BR, Friedmann Angeli JP, Bayir H, et al. Ferroptosis: A Regulated Cell Death Nexus Linking Metabolism, Redox Biology, and Disease. Cell. 2017 Oct 5;171(2):273-285. doi: 10.1016/j.cell.2017.09.021. PMID: 28985560; PMCID: PMC5685180.

[7]. Chen X, Li J, Kang R, et al. Ferroptosis: machinery and regulation. Autophagy. 2021 Sep;17(9):2054-2081. doi: 10.1080/15548627.2020.1810918. Epub 2020 Aug 26. PMID: 32804006; PMCID: PMC8496712.

[8]. Friedmann Angeli JP, Krysko DV, Conrad M. Ferroptosis at the crossroads of cancer-acquired drug resistance and immune evasion. Nat Rev Cancer. 2019 Jul;19(7):405-414. doi: 10.1038/s41568-019-0149-1. PMID: 31101865.

[9]. Yang WS, SriRamaratnam R, Welsch ME, et al. Regulation of ferroptotic cancer cell death by GPX4. Cell. 2014 Jan 16;156(1-2):317-331. doi: 10.1016/j.cell.2013.12.010. PMID: 24439385; PMCID: PMC4076414.

[10]. Wang Y, Zheng L, Shang W, et al. Wnt/beta-catenin signaling confers ferroptosis resistance by

targeting GPX4 in gastric cancer. Cell Death Differ. 2022 Nov;29(11):2190-2202. doi: 10.1038/s41418-022-01008-w. Epub 2022 May 9. PMID: 35534546; PMCID: PMC9613693.

[11]. Viswanathan VS, Ryan MJ, Dhruv HD, et al. Dependency of a therapy-resistant state of cancer cells on a lipid peroxidase pathway. Nature. 2017 Jul 27;547(7664):453-457. doi: 10.1038/nature23007. Epub 2017 Jul 5. PMID: 28678785; PMCID: PMC5667900.

[12]. Zhou J, Tong F, Zhao J, et al. Identification of the E2F1-RAD51AP1 axis as a key factor in MGMT-methylated GBM TMZ resistance. Cancer Biol Med. 2023 Jun 5;20(5):385–400. doi: 10.20892/j.issn.2095-3941.2023.0011. PMID: 37283490; PMCID: PMC10246439.

[13]. Kuo LJ, Yang LX. Gamma-H2AX - a novel biomarker for DNA double-strand breaks. In Vivo. 2008 May-Jun;22(3):305-9. PMID: 18610740.

[14]. Jette NR, Radhamani S, Arthur G, Ye R, Goutam S, Bolyos A, Petersen LF, Bose P, Bebb DG, Lees-Miller SP. Combined poly-ADP ribose polymerase and ataxia-telangiectasia mutated/Rad3-related inhibition targets ataxia-telangiectasia mutated-deficient lung cancer cells. Br J Cancer. 2019 Oct;121(7):600-610. doi: 10.1038/s41416-019-0565-8. Epub 2019 Sep 4. Erratum in: Br J Cancer. 2020 Apr 17;: PMID: 31481733; PMCID: PMC6889280.

[15]. Sharma A, Singh K, Almasan A. Histone H2AX phosphorylation: a marker for DNA damage. Methods Mol Biol. 2012;920:613-26. doi: 10.1007/978-1-61779-998-3_40. PMID: 22941631.

[16]. Chi H, Li B, Wang Q, et al. Opportunities and challenges related to ferroptosis in glioma and neuroblastoma. Front Oncol. 2023 Mar 2;13:1065994. doi: 10.3389/fonc.2023.1065994. PMID: 36937406; PMCID: PMC10021024.

[17]. Lee SY. Temozolomide resistance in glioblastoma multiforme. Genes Dis. 2016 May 11;3(3):198-210. doi: 10.1016/j.gendis.2016.04.007. PMID: 30258889; PMCID: PMC6150109.

[18]. Kao TJ, Lin CL, Yang WB, et al. Dysregulated lipid metabolism in TMZ-resistant glioblastoma: pathways, proteins, metabolites and therapeutic opportunities. Lipids Health Dis. 2023 Aug 3;22(1):114. doi: 10.1186/s12944-023-01881-5. PMID: 37537607; PMCID: PMC10398973.

[19]. Jiapaer S, Furuta T, Tanaka S, et al. Potential Strategies Overcoming the Temozolomide Resistance for Glioblastoma. Neurol Med Chir (Tokyo). 2018 Oct 15;58(10):405-421. doi: 10.2176/nmc.ra.2018-0141. Epub 2018 Sep 21. PMID: 30249919; PMCID: PMC6186761.

[20]. Jatyan R, Singh P, Sahel DK, Karthik YG, Mittal A, Chitkara D. Polymeric and small molecule-conjugates of temozolomide as improved therapeutic agents for glioblastoma

multiforme. J Control Release. 2022 Oct;350:494-513. doi: 10.1016/j.jconrel.2022.08.024. Epub 2022 Sep 1. PMID: 35985493.

[21]. Wan S, Zhang G, Liu R, et al. Pyroptosis, ferroptosis, and autophagy cross-talk in glioblastoma opens up new avenues for glioblastoma treatment. Cell Commun Signal. 2023 May 19;21(1):115. doi: 10.1186/s12964-023-01108-1. PMID: 37208730; PMCID: PMC10199557.

[22]. Shaw P, Kumar N, Privat-Maldonado A, et al. Cold Atmospheric Plasma Increases Temozolomide Sensitivity of Three-Dimensional Glioblastoma Spheroids via Oxidative Stress-Mediated DNA Damage. Cancers (Basel). 2021 Apr 8;13(8):1780. doi: 10.3390/cancers13081780. PMID: 33917880; PMCID: PMC8068248.

[23]. Chen TC, Chuang JY, Ko CY, et al. AR ubiquitination induced by the curcumin analog suppresses growth of temozolomide-resistant glioblastoma through disrupting GPX4-Mediated redox homeostasis. Redox Biol. 2020 Feb;30:101413. doi: 10.1016/j.redox.2019.101413. Epub 2019 Dec 26. PMID: 31896509; PMCID: PMC6940696.

[24]. Viswanathan VS, Ryan MJ, Dhruv HD, et al. Dependency of a therapy-resistant state of cancer cells on a lipid peroxidase pathway. Nature. 2017 Jul 27;547(7664):453-457. doi: 10.1038/nature23007. Epub 2017 Jul 5. PMID: 28678785; PMCID: PMC5667900.

[25]. Yang WS, SriRamaratnam R, Welsch ME, et al. Regulation of ferroptotic cancer cell death by GPX4. Cell. 2014 Jan 16;156(1-2):317-331. doi: 10.1016/j.cell.2013.12.010. PMID: 24439385; PMCID: PMC4076414.

[26]. Dixon SJ, Lemberg KM, Lamprecht MR, et al. Ferroptosis: an iron-dependent form of nonapoptotic cell death. Cell. 2012 May 25;149(5):1060-72. doi: 10.1016/j.cell.2012.03.042. PMID: 22632970; PMCID: PMC3367386.

[27]. Xu T, Ding W, Ji X, et al. Molecular mechanisms of ferroptosis and its role in cancer therapy. J Cell Mol Med. 2019 Aug;23(8):4900-4912. doi: 10.1111/jcmm.14511. Epub 2019 Jun 24. PMID: 31232522; PMCID: PMC6653007.

[28]. Cao JY, Dixon SJ. Mechanisms of ferroptosis. Cell Mol Life Sci. 2016 Jun;73(11-12):2195-209. doi: 10.1007/s00018-016-2194-1. Epub 2016 Apr 5. PMID: 27048822; PMCID: PMC4887533.

[29]. Forcina GC, Dixon SJ. GPX4 at the Crossroads of Lipid Homeostasis and Ferroptosis. Proteomics. 2019 Sep;19(18):e1800311. doi: 10.1002/pmic.201800311. Epub 2019 May 31.

PMID: 30888116.

[30]. Gao M, Yi J, Zhu J, et al. Role of Mitochondria in Ferroptosis. Mol Cell. 2019 Jan 17;73(2):354-363.e3. doi: 10.1016/j.molcel.2018.10.042. Epub 2018 Dec 20. PMID: 30581146; PMCID: PMC6338496.

[31]. Chi H, Li B, Wang Q, et al. Opportunities and challenges related to ferroptosis in glioma and neuroblastoma. Front Oncol. 2023 Mar 2;13:1065994. doi: 10.3389/fonc.2023.1065994. PMID: 36937406; PMCID: PMC10021024.